LETTER

doi:10.1038/nature11431

Controlling interneuron activity in *Caenorhabditis elegans* to evoke chemotactic behaviour

Askin Kocabas[1,2]*, Ching-Han Shen[1,2]*, Zengcai V. Guo[3] & Sharad Ramanathan[1,2,4,5,6]

Animals locate and track chemoattractive gradients in the environment to find food. With its small nervous system, *Caenorhabditis elegans* is a good model system[1,2] in which to understand how the dynamics of neural activity control this search behaviour. Extensive work on the nematode has identified the neurons that are necessary for the different locomotory behaviours underlying chemotaxis through the use of laser ablation[3–7], activity recording in immobilized animals and the study of mutants[4,5]. However, we do not know the neural activity patterns in *C. elegans* that are sufficient to control its complex chemotactic behaviour. To understand how the activity in its interneurons coordinate different motor programs to lead the animal to food, here we used optogenetics and new optical tools to manipulate neural activity directly in freely moving animals to evoke chemotactic behaviour. By deducing the classes of activity patterns triggered during chemotaxis and exciting individual neurons with these patterns, we identified interneurons that control the essential locomotory programs for this behaviour. Notably, we discovered that controlling the dynamics of activity in just one interneuron pair (AIY) was sufficient to force the animal to locate, turn towards and track virtual light gradients. Two distinct activity patterns triggered in AIY as the animal moved through the gradient controlled reversals and gradual turns to drive chemotactic behaviour. Because AIY neurons are post-synaptic to most chemosensory and thermosensory neurons[8], it is probable that these activity patterns in AIY have an important role in controlling and coordinating different taxis behaviours of the animal.

Organisms, from bacteria to multicellular eukaryotes, have to search for food to survive. Complex internal circuits process external signals to evoke and coordinate multiple motor programs, leading the animal to track attractive odours and find food. Whether there are master nodes in the circuits that control and coordinate search behaviour, and whether the neural circuits generating chemotactic behaviour in *C. elegans* can be controlled through such key nodes are important questions.

The nematode *C. elegans* uses reversals (backward movement) and sharp and gradual turns to locate and track gradients of chemoattractive

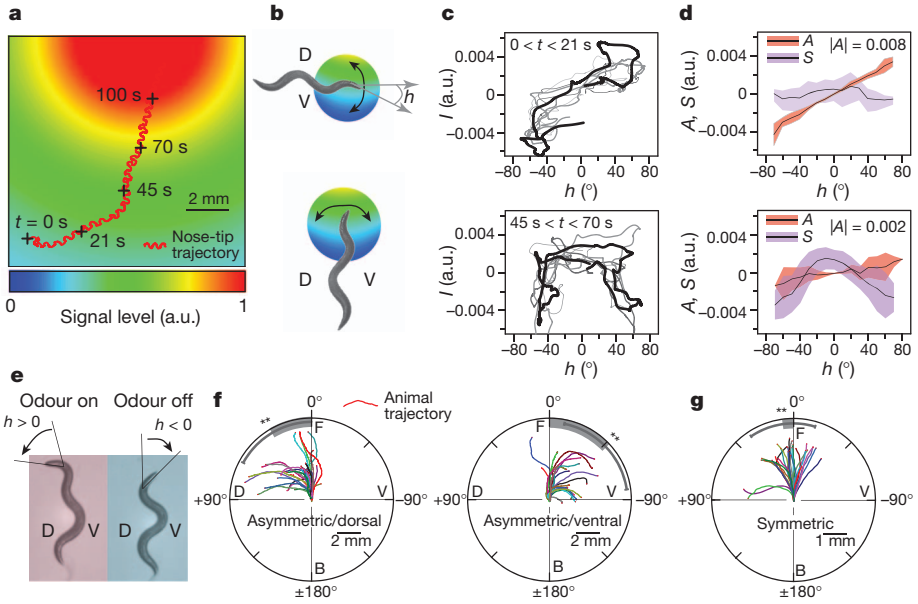

Figure 1 | Asymmetric component of the odour signal controls gradual turning. a, The trajectory of the nose tip of a nematode overlaid on a modelled exponential profile (decay length, 1 cm) of the gradient of chemoattractants (pseudocolour) from the bacterial lawn. Plus signs denote the position of the animal at the indicated times. a.u., arbitrary units. **b**, Illustrations of an animal crawling perpendicular to (top) and along (bottom) the odour gradient. *h*, head-bending angle; D, dorsal ($h > 0$); V, ventral ($h < 0$). **c**, Odour signal at nose tip, $I(t)$, versus head-bending angle, $h(t)$, over the last (black) and sequentially earlier (grey) head swings for the nose-tip trajectory in **a**. **d**, Plot of the mean (black line) and s.d. (coloured bar) of the asymmetric (A) and symmetric (S) components of $I(t)$ in **c**. $|A|$ denotes the magnitude of $A(t)$. **e**, Dorsal asymmetric odour stimulation (see Methods). **f**, **g**, Sample trajectories of the centre of mass of the animals upon dorsal and ventral asymmetric (**f**) and symmetric (**g**) odour stimulation. Angles define the turning angles with respect to the initial orientation of the animal. Grey bar denotes the mean and error bars denote s.d. over $n = 10$ experiments. B, back; F, front. $^{**}P < 0.05$, two-sample *t*-test.

[1]FAS Center for Systems Biology, Harvard University, Cambridge, Massachusetts 02138, USA. [2]Department of Molecular and Cellular Biology, Harvard University, Cambridge, Massachusetts 02138, USA. [3]Janelia Farm Research Campus, Howard Hughes Medical Institute, Ashburn, Virginia 20147, USA. [4]Allen Institute for Brain Science, Seattle, Washington 98103, USA. [5]Harvard Stem Cell Institute, Harvard University, Cambridge, Massachusetts 02138, USA. [6]School of Engineering and Applied Sciences, Harvard University, Cambridge, Massachusetts 02138, USA.
*These authors contributed equally to this work.

signals[4,5,9,10]. Previous work on *C. elegans* has identified around 14 pairs of interneurons and motor neurons, including the interneuron pairs AIY, AIZ and AIB that are necessary for the locomotory behaviours underlying chemotaxis[3–7] (Supplementary Table 1). The neuroanatomy of the animal shows that most of the amphid chemosensory and thermosensory neurons synapse onto one or more neurons of the first layer of the interneuron pairs AIY, AIZ and AIB[11], which are further connected to a dense network of interneurons[8]. The activity dynamics in this network must process sensory signals to produce and coordinate the different locomotory behaviours underlying chemotaxis through the downstream motor neurons. Despite the experiments in the literature involving ablation, genetics and calcium imaging, we do not know whether chemotaxis is driven by key interneurons or whether the generation of this complex behaviour is achieved by the dynamics of a more diffuse neural network.

To evoke chemotactic behaviour by directly controlling interneuron activity, we have to answer the intricately linked questions of which sets of interneurons to control, and which activity patterns to stimulate in them. To deduce the classes of activity patterns triggered in the nervous system during chemotaxis, we followed animals as they crawled towards a bacterial lawn (Fig. 1a). The undulatory head swings (from dorsal to ventral, as the animal crawls on its side) caused the angle at which the head bends relative to the locomotory direction, $h(t)$ (Fig. 1b), to oscillate between positive and negative values. Owing to this changing head-bending angle and the movement of the animal, sensory cilia at the nose tip experienced the spatial profile of the chemoattractants (Fig. 1a, b) as a temporally fluctuating odour signal, $I(h,t)$. In general, this signal can be written as a sum of two terms, $I(h,t) = S_I(h,t) + A_I(h,t)$, in which S_I is a symmetric function of h: $S(h,t) = S(-h,t)$ and A_I is an asymmetric function of h:

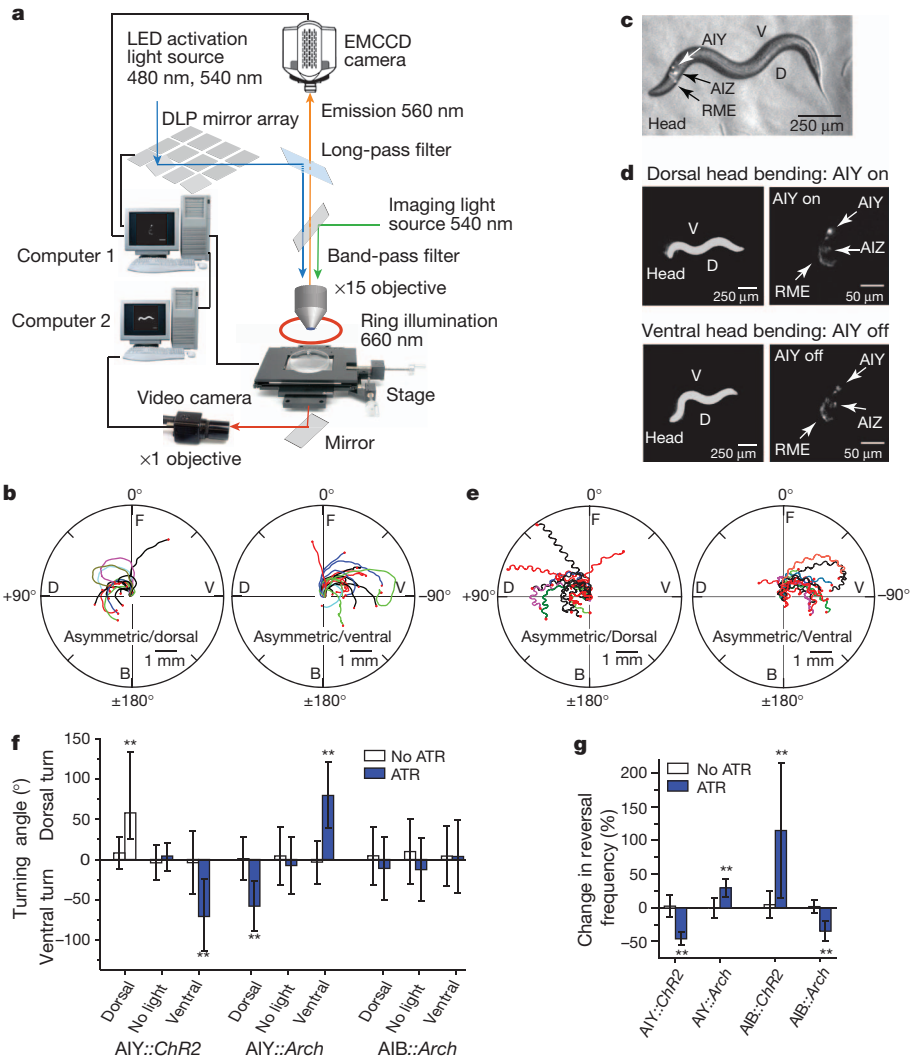

Figure 2 | Asymmetric and symmetric excitation of AIY control gradual turning and reversal frequency. **a**, Set-up for closed-loop single-neuron stimulation (see Methods). DLP, digital light processing; EMCCD, electron-multiplying charge-coupled device; LED, light-emitting diode. **b**, Sample trajectories of the centre of mass of the animals after dorsal or ventral asymmetric excitation of AIY ($n = 10$; *ttx-3::ChR2*). **c**, Fluorescence image overlaid on the bright-field image of a nematode co-expressing ChR2 and mKO in AIY, AIZ and RME neurons (*ser-2prom2::mKO* and *ser-2prom2::ChR2*). **d**, Asymmetric dorsal stimulation of the animal in **c**. On dorsal head bending (top left), ChR2 and mKO were excited in AIY using the set-up in **a** (top right, higher fluorescence in AIY) but not on ventral head bending (bottom right, decreased fluorescence in AIY). Left, ×1 dark-field images of the animal; right, ×15 fluorescent images of the neurons in the same animal. **e**, Sample trajectories of the nose tip of the animals on dorsal (left) or ventral (right) asymmetric excitation of AIY ($n = 10$; *ser-2prom2::ChR2*). **f**, Turning angle of animals after asymmetric stimulation of AIY::*ChR2* ($n = 10$), AIY::*Arch* ($n = 10$) and AIB::*Arch* ($n = 7$). ATR, all-*trans* retinal (co-factor required for functional light-gated channels *ChR2* and *Arch*). 'Dorsal' indicates asymmetric dorsal stimulation, 'ventral' indicates asymmetric ventral stimulation, 'no light' indicates unstimulated neurons, and 'no ATR' indicates control experiments. **g**, Reversal frequencies upon symmetric stimulation of AIY::*ChR2* ($n = 10$), AIY::*Arch* ($n = 19$), AIB::*ChR2* ($n = 14$) and AIB::*Arch* ($n = 11$). White and blue bars in **f** and **g** denote the mean, error bars denote 1 s.d. over n animals. $^{**}P < 0.05$, two-sample t-test).

$A(h,t) = -A(-h,t)$. When the animal moves perpendicular to the gradient direction, I is dominated by A_I (Fig. 1b–d, top). As the animal turns and tracks the gradient, the magnitude of A_I, $|A_I|$ decreases and I is dominated by S_I (Fig. 1b–d, bottom and Supplementary Fig. 1a).

To determine how these asymmetric and symmetric components of $I(t)$ control locomotory behaviour, we built a microscopy system that delivers odours on a freely crawling animal in precise temporal patterns determined by $h(t)$ (Supplementary Fig. 1b). To mimic A_I, we exposed the animal to asymmetric odour stimulation: air with chemoattractant vapours (1×10^{-3} M isoamyl alcohol) blown on the entire animal when the head was bent in one direction (for example, dorsally, $h > 0$) and odour-free air blown when the head was bent in the other direction (ventrally, $h < 0$) (Fig. 1e). The animal turned gradually in the direction in which its head was bent when the odour was delivered (Fig. 1f, Supplementary Fig. 1c, d and Supplementary Movie 1). To mimic S_I, we delivered vapours of isoamyl alcohol constantly, independent of h. The animal reduced its reversal frequency[11] and did not turn (Fig. 1g). The most parsimonious hypothesis based on these results is that asymmetric and symmetric odour components generate activity patterns in the nervous system with corresponding symmetries to control turning and reversal frequency separately during chemotaxis.

We therefore identified interneurons that triggered the different locomotory behaviours necessary for chemotaxis by directly stimulating individual neurons in a freely moving animal in asymmetric and symmetric patterns. To do so, we expressed channelrhodopsin-2 (ChR2)[12,13] or archaerhodopsin-3 (Arch)[14,15] in different neurons. Light activation of ChR2 (by 480 nm light) and Arch (540 nm) leads to neural excitation and inhibition, respectively.

Targeted illumination of specific neurons in motionless animals[16] and of body segments in freely moving animals[17,18] have been developed to excite neurons for which specific promoters are not known. Because the neurons in the nerve ring are as close as 5–10 μm to each other and their relative positions change quickly as

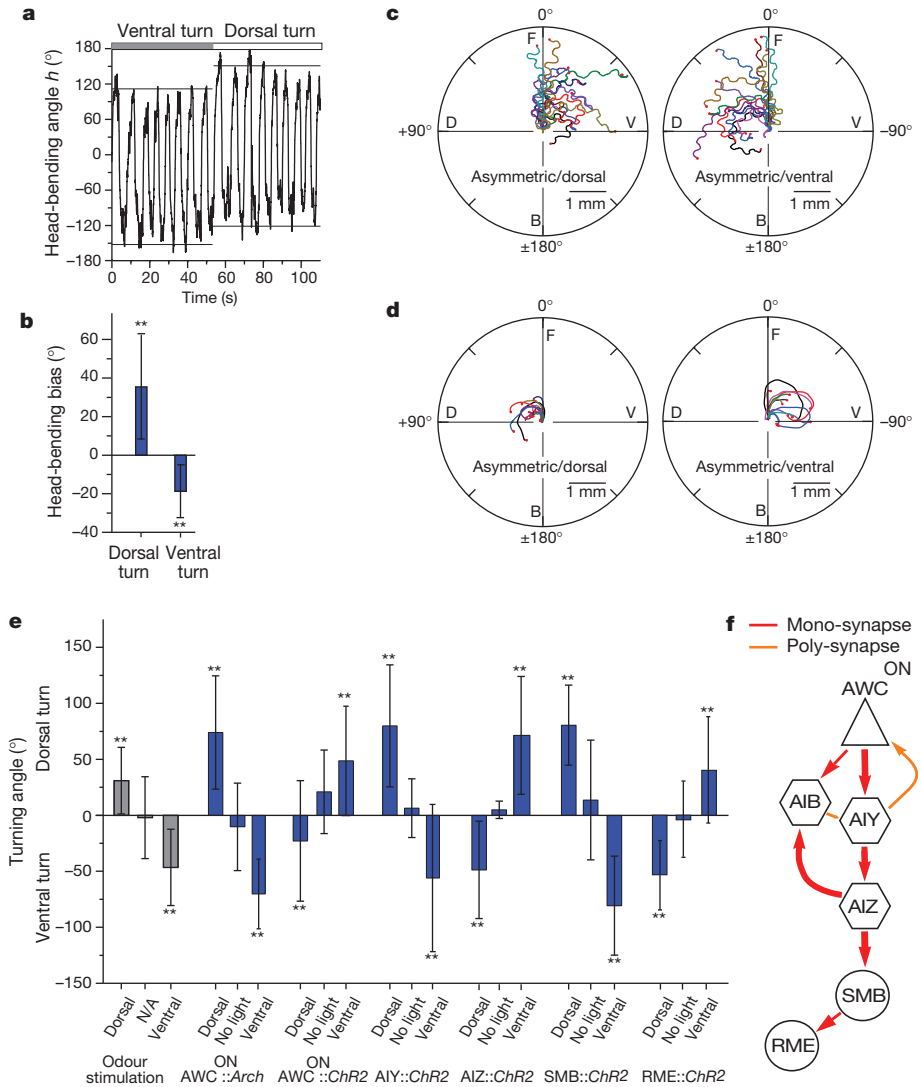

Figure 3 | Asymmetric AIY excitation modulates the head-bending angle to cause turning. **a**, Representative head-bending angle (horizontal lines denote means of maximum and minimum h during each full head swing) of an *AIY::ChR2* (*ttx-3::ChR2*) animal forced to first turn ventrally and then dorsally (positive angles, dorsal; negative angles, ventral). **b**, Histogram of head-bending angle bias ($\max(h) + \min(h)$) during dorsal and ventral turn caused by asymmetric AIY excitation. Error bars denote s.d. over $n = 5$. **c**, **d**, Sample tracks of animals on dorsal (left) or ventral (right) asymmetric excitation of AIZ::*ChR2* (*ser-2prom2::ChR2*) (**c**), and SMB::*ChR2* (*odr-2(18)::ChR2*) (**d**) animals. **e**, Turning angle upon asymmetric stimulation with odour ($n = 10$) and optically of AWC^{ON}::*Arch* ($n = 10$), AWC^{ON}::*ChR2* ($n = 9$), AIY::*ChR2* ($n = 10$), AIZ::*ChR2* ($n = 5$), SMB::*ChR2* ($n = 5$) and RME::*ChR2* ($n = 5$). 'Dorsal' indicates asymmetric dorsal stimulation, 'ventral' indicates asymmetric ventral stimulation and 'no light' indicates unstimulated neurons. Error bars denote s.d. over n. $^{**}P < 0.05$, two-sample t-test. **f**, The mono- and polysynapses between AWC^{ON}, AIY, AIB, AIZ, SMB and RME (thickness of arrows is proportional to synapse number). Triangle denotes sensory neuron, hexagons denote interneuron and circles denote motor neurons.

the animal moves (Supplementary Fig. 2a), we could not use these techniques. To stimulate one of many neurons optically (each with a diameter of 5–10 μm) expressing light-gated ion channels in the nerve ring of an animal that typically moves at 150 ± 50 μm s^{-1} (Supplementary Fig. 2b), our set-up tracks, identifies and specifically illuminates the neuron(s) of interest, all within 25 ms, to achieve a 5-μm spatial resolution of excitation (Fig. 2a).

Using this set-up, we first tested how stimulating the interneurons AIY and AIB affected locomotory behaviour. Both neuron pairs receive chemical synapses from the AWC sensory neurons that detect isoamyl alcohol[8] and showed calcium activity when animals were stimulated with this chemoattractant[11]. Asymmetric excitation of AIY with light in animals that expressed ChR2 only in AIY (under the promoter *ttx-3*) caused the animal to turn in the direction in which the head was bent when AIY were excited (Fig. 2b and Supplementary Movie 2). We validated our set-up by reproducing these results in animals that expressed ChR2 in AIY alone and the fluorescent protein monomeric Kusabira-Orange (mKO) in neurons AIY, AIZ and RME (under the promoter *ser-2prom2*, Supplementary Fig. 2c–f). Asymmetric stimulation of AIY in animals expressing ChR2 in AIY, AIZ and RME (*ser-2prom2*) showed the same results (Fig. 2c–f, Supplementary Fig. 2g and Supplementary Movie 3). Consistently, inhibiting the activity in AIY asymmetrically (*ttx-3::Arch*) caused the animal to turn in the opposite direction in which the head was bent when AIY were inhibited (Fig. 2f, Supplementary Fig. 3a and Supplementary Movie 4). Symmetric excitation and inhibition of AIY decreased and increased the reversal frequency respectively, but did not cause turning (Fig. 2g, Supplementary Fig. 3 and Supplementary Movie 5).

Both asymmetric and symmetric excitation or inhibition of AIB in AIB::*ChR2* and AIB::*Arch* animals (in which *ChR2* and *Arch* are expressed under the *npr-9* promoter) affected the reversal frequency of the animal but did not produce any gradual turning (Fig. 2f, g and Supplementary Fig. 4). We could thus control the two locomotory behaviours crucial for chemotaxis—gradual turns and reversal frequency—by driving different patterns of activity in AIY alone.

Turning is initiated by a larger head-bending angle in one direction[19,20]. When we forced the animal to turn by asymmetrically stimulating AIY (*ttx-3::ChR2*), the head-bending angle in the direction of the turn increased (Fig. 3a, b), indicating that asymmetric activation of AIY controlled head bending through head motor neurons to cause gradual turning. AIY neurons are most directly connected to the head muscles through the interneuron pair AIZ, which synapse onto the head motor neurons SMB and RME[8]. AIZ neurons have been proposed to have a role in gradual turns by laser ablation[4]. Ablations of SMB and RME change the head-bending angle during crawling and show loopy behaviour[7,21].

When we specifically excited AIZ::*ChR2* (*ser-2prom2::ChR2*), SMB::*ChR2* (*odr-2(18)::ChR2*) or RME::*ChR2* (*ser-2prom2::ChR2*) asymmetrically using our set-up, the animals turned (Fig. 3c–e, Supplementary Fig. 5 and Supplementary Movies 6–8). These results, in conjunction with those from asymmetric optical stimulation of the isoamyl-alcohol-sensing neuron AWC^{ON} (Supplementary Fig. 6 and Supplementary Movie 9), show that asymmetric stimulation of the sequence of anatomically connected neurons from AWC^{ON}, through the interneurons AIY and AIZ to the head motor neurons SMB and RME[8] (Fig. 3f) all cause turning. These sets of neurons thus sense and respond to the component of the sensory signal that oscillates asymmetrically and in synchrony with head movement to control head bending and turning.

As different patterns of activity in AIY are sufficient to control both the frequency of reversals and turning, we tested whether controlling AIY activity alone was sufficient to coordinate reversal frequency and turning to evoke chemotactic behaviour. To do so, we measured the

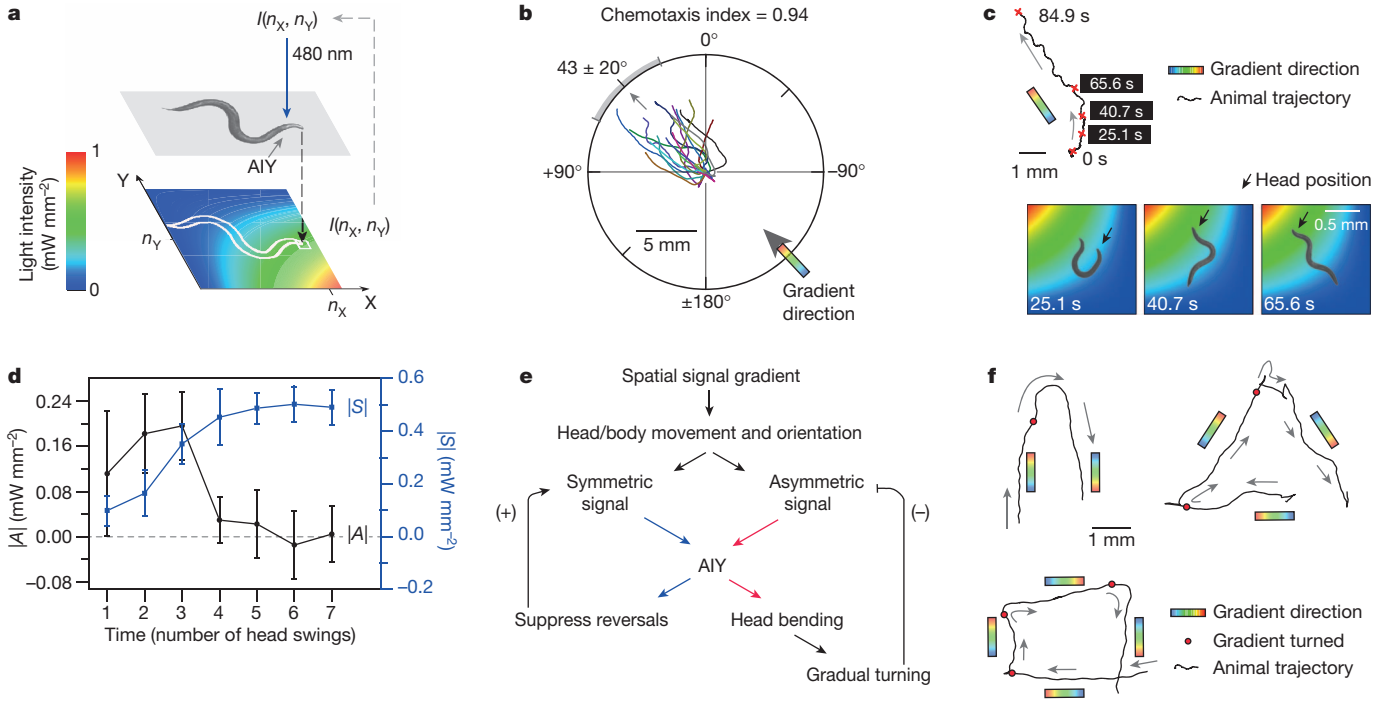

Figure 4 | Controlling AIY activity is sufficient to evoke chemotactic behaviour. **a**, Virtual light gradient algorithm (see Methods). At each time, *t*, AIY::*ChR2* animals (*ttx-3::ChR2*) are stimulated with 480 nm blue light with an intensity ($I(n_x,n_y)$) of the virtual gradient at the nose-tip position (n_x,n_y). **b**, Trajectories of AIY::*ChR2* animals moving in a virtual light gradient (as in **a**) with a gradient direction at 45° (black arrowheads denote the mean direction of the trajectory. Grey bar denotes s.d. ($n = 10$). **c**, Top, a sample trajectory of an animal in **b**. Bottom, snapshots of the animal making a gradual turn to reorient itself to the gradient direction (pseudocolor, same as **a**). **d**, Magnitude of A_1 (black) and S_1 (blue, right axis), over a head swing, as a function of the number of head swings during a gradual turn ($n = 5$, from trajectories in **b**, error bar denotes 1 s.d.). **e**, Model for chemotaxis in the virtual light gradient. **f**, Trajectories of the centre of mass of the animals when the gradient direction was suddenly rotated (at times when the animal reached the red dots) by 180°, 120° or 90°.

locomotory behaviour of animals in a fixed spatial light gradient that directly excited AIY::*ChR2* (Supplementary Fig. 7a and Supplementary Methods). The animals were unable to track the gradient direction (Supplementary Fig. 7c and Supplementary Movie 10).

The somas and processes of AIY are 150 ± 25 μm behind the nose tip of an adult animal (Supplementary Fig. 7b). As the speed of the animal is $150 \pm 50\ \mu m\ s^{-1}$, AIY neurons follow the position of the nose tip with approximately a 1-second delay. We proposed that the dynamics of AIY excitation caused by the movement of the animal through the gradient were not in synchrony with head bending due to this delay, preventing the animals from tracking the gradient. Therefore, we designed a virtual light gradient in which the excitation light intensity on AIY depended not on the positions of AIY in space but on the position of the nose tip (Fig. 4a, Supplementary Fig. 7a and Supplementary Methods).

In this set-up, animals changed their locomotory direction using reversals and gradual turns to track the gradient direction stably (the fraction of the animals moving up the gradient and hence to the correct quadrant (defined as chemotaxis index[22]) = 0.94, Fig. 4b). As with the odour profile at the nose tip (Fig. 1d), the temporal light-intensity pattern that excited AIY could be written as a sum of an asymmetric ($A_I(h,t)$) and a symmetric ($S_I(h,t)$) component. When the locomotory direction of the animal was not along the direction of the light gradient, the magnitude of $A_I(h,t)$ over each head swing, $|A| = \sqrt{\langle A_I^2(h,t)\rangle}$, was larger, exciting AIY asymmetrically to make the animal turn. As the animal oriented itself along the direction of the gradient, the magnitude of $A_I(h,t)$ continuously diminished, suppressing turns, whereas the magnitude of $S_I(h,t)$, $|S|$, increased and suppressed reversals (Fig. 4c, d). Thus, manipulating the dynamics of activity in just the AIY interneuron pair is sufficient to evoke chemotactic behaviour. This is because the head bending and locomotion of the animal through the virtual light gradient together generate and modulate the levels of symmetric and asymmetric excitation of AIY which, in turn, control future locomotory behaviour (Fig. 4e).

This model would predict robust chemotactic behaviour in the light gradient stimulating AIY, with the symmetric and asymmetric components modulating their relative magnitudes to guide the animal stably in the correct direction. To test for robust tracking, we suddenly rotated the virtual light gradient direction by different angles and measured the response of the animal. The animals followed the gradient direction as this direction was suddenly and repeatedly rotated by 180° (Supplementary Movie 11), 120° or 90° (Fig. 4f).

Previous studies have identified neurons involved in chemotaxis by showing that defects in these neurons compromise locomotory programs and sensory modalities necessary for this behaviour. Through our approach we can identify key neurons in the neural network, the dynamics of which are sufficient to drive chemotactic behaviour and hence act as control nodes in the network. Our study leads to questions of how activity patterns stimulated in the AIY neurons during chemotaxis are disentangled by the downstream neurons to drive the different motor programs. Because many chemosensory and thermosensory neurons synapse onto AIY interneurons, it is likely that the modulation of symmetric and asymmetric activity patterns in these interneurons have a central role in the different taxis behaviours of *C. elegans*. Our techniques provide avenues to identify and generate neural activity patterns to control all of the behaviours of this nematode.

METHODS SUMMARY

Transgenic lines were constructed[2] in the *pha-1* (ref. 22) and *lite-1* (ref. 23) background and maintained using standard molecular biology techniques (see Methods). The details of the data analysis to quantify chemotactic behaviour, reversal frequency and the set-up for odour stimulation, single neuron stimulation and virtual light gradients are explained in Methods.

Full Methods and any associated references are available in the online version of the paper.

Received 17 May; accepted 23 July 2012.
Published online 23 September 2012.

1. Brenner, S. The genetics of behaviour. *Br. Med. Bull.* **29,** 269–271 (1973).
2. Brenner, S. The genetics of *Caenorhabditis elegans*. *Genetics* **77,** 71–94 (1974).
3. Tsalik, E. L. & Hobert, O. Functional mapping of neurons that control locomotory behavior in *Caenorhabditis elegans*. *J. Neurobiol.* **56,** 178–197 (2003).
4. Iino, Y. & Yoshida, K. Parallel use of two behavioral mechanisms for chemotaxis in *Caenorhabditis elegans*. *J. Neurosci.* **29,** 5370–5380 (2009).
5. Pierce-Shimomura, J. T., Morse, T. M. & Lockery, S. R. The fundamental role of pirouettes in *Caenorhabditis elegans* chemotaxis. *J. Neurosci.* **19,** 9557–9569 (1999).
6. Wakabayashi, T., Kitagawa, I. & Shingai, R. Neurons regulating the duration of forward locomotion in *Caenorhabditis elegans*. *Neurosci. Res.* **50,** 103–111 (2004).
7. Gray, J. M., Hill, J. J. & Bargmann, C. I. A circuit for navigation in *Caenorhabditis elegans*. *Proc. Natl Acad. Sci. USA* **102,** 3184–3191 (2005).
8. White, J. G., Southgate, E., Thomson, J. N. & Brenner, S. The structure of the nervous system of the nematode *Caenorhabditis elegans*. *Phil. Trans. R. Soc. Lond. B* **314,** 1–340 (1986).
9. Ward, S. Chemotaxis by the nematode *Caenorhabditis elegans*: identification of attractants and analysis of the response by use of mutants. *Proc. Natl Acad. Sci. USA* **70,** 817–821 (1973).
10. Izquierdo, E. J. & Lockery, S. R. Evolution and analysis of minimal neural circuits for klinotaxis in *Caenorhabditis elegans*. *J. Neurosci.* **30,** 12908–12917 (2010).
11. Chalasani, S. H. *et al.* Dissecting a circuit for olfactory behaviour in *Caenorhabditis elegans*. *Nature* **450,** 63–70 (2007).
12. Boyden, E. S., Zhang, F., Bamberg, E., Nagel, G. & Deisseroth, K. Millisecond-timescale, genetically targeted optical control of neural activity. *Nature Neurosci.* **8,** 1263–1268 (2005).
13. Nagel, G. *et al.* Light activation of channelrhodopsin-2 in excitable cells of *Caenorhabditis elegans* triggers rapid behavioral responses. *Curr. Biol.* **15,** 2279–2284 (2005).
14. Chow, B. Y. *et al.* High-performance genetically targetable optical neural silencing by light-driven proton pumps. *Nature* **463,** 98–102 (2010).
15. Okazaki, A., Sudo, Y. & Takagi, S. Optical silencing of *C. elegans* cells with arch proton pump. *PLoS ONE* **7,** e35370 (2012).
16. Guo, Z. V., Hart, A. C. & Ramanathan, S. Optical interrogation of neural circuits in *Caenorhabditis elegans*. *Nature Methods* **6,** 891–896 (2009).
17. Leifer, A. M., Fang-Yen, C., Gershow, M., Alkema, M. J. & Samuel, A. D. T. Optogenetic manipulation of neural activity in freely moving *Caenorhabditis elegans*. *Nature Methods* **8,** 147–152 (2011).
18. Stirman, J. N. *et al.* Real-time multimodal optical control of neurons and muscles in freely behaving *Caenorhabditis elegans*. *Nature Methods* **8,** 153–158 (2011).
19. Lockery, S. R. The computational worm: spatial orientation and its neuronal basis in *C. elegans*. *Curr. Opin. Neurobiol.* **21,** 782–790 (2011).
20. Kim, D., Park, S., Mahadevan, L. & Shin, J. H. The shallow turn of a worm. *J. Exp. Biol.* **214,** 1554–1559 (2011).
21. McIntire, S. L., Jorgensen, E., Kaplan, J. & Horvitz, H. R. The GABAergic nervous system of *Caenorhabditis elegans*. *Nature* **364,** 337–341 (1993).
22. Granato, M., Schnabel, H. & Schnabel, R. *pha-1*, a selectable marker for gene transfer in *C. elegans*. *Nucleic Acids Res.* **22,** 1762–1763 (1994).
23. Edwards, S. L. *et al.* A novel molecular solution for ultraviolet light detection in *Caenorhabditis elegans*. *PLoS Biol.* **6,** e198 (2008).

Supplementary Information is available in the online version of the paper.

Acknowledgements We thank J. Dowling, S. Lockery, J. Lichtman, K. McCormick, A. Murray, E. O'Shea, A. Schier, B. Stern and members of the Ramanathan laboratory for discussions and comments, the Human Frontier Science Program (HFSP) Postdoctoral Fellowship (A.K.), National Science Foundation (NSF) Graduate Fellowship (C.-H.S.), NSF Career Award, Pew Scholar, Klingenstein Fellowship Award and the National Institutes of Health (NIH) Pioneer Awards (S.R.) for support.

Author Contributions A.K., C.-H.S., Z.V.G. and S.R. designed the experiments. A.K., C.-H.S. and Z.V.G. performed the experiments. A.K., C.-H.S. and S.R. wrote the manuscript.

Author Information Reprints and permissions information is available at www.nature.com/reprints. The authors declare no competing financial interests. Readers are welcome to comment on the online version of the paper. Correspondence and requests for materials should be addressed to A.K. (akocabas@cgr.harvard.edu) or S.R. (sharad@post.harvard.edu).

METHODS

Strains were grown and maintained under standard conditions[2] unless indicated otherwise. Transgenic lines with a *pha-1* selection marker were grown at 24 °C (ref. 22). All optical stimulation experiments were done in *lite-1* mutants to minimize the sensitivity of the animal to blue light[23]. A complete strain list and information on transgenes are included in Supplementary Table 2.

Chemotaxis analysis. Animal chemotaxis towards a bacterial lawn was assayed on an open-lid, 10-cm nematode growth medium (NGM) plate incubated at room temperature (22 °C) overnight with 10 µl *Escherichia coli* strain OP50 at the centre. N2 strain young adults were placed on the plate 1.5 cm away from the centre of the bacterial lawn. Animal behaviour was recorded under ×6 magnification by an EMCCD camera at 20 Hz and analysed by customized LabView scripts.

Odour-stimulation set-up. An N2 young adult was placed on an open-lid, food-free 10-cm NGM plate for at least 1 min. An electric valve (Supplementary Fig. 1b) was used to determine whether the air (100 standard cubic centimetres per minute (s.c.c.m.)) was bubbled through water or 1×10^{-3} M isoamyl alcohol on the basis of the posture of the freely moving animal. The images were recorded under ×6 magnification by an EMCCD camera at 20 Hz and analysed by customized LabView scripts.

Single-neuron stimulation set-up. L4-stage animals were transferred to a new NGM plate with a thin layer of *E. coli* OP50, containing 100 µM ATR[16] if required, 24 h before experiments in room temperature. An animal then was placed on an open-lid, food-free 6-cm NGM plate for at least 1 min. Dark-field 660 nm illumination was used to visualize the posture of the animal under ×1 magnification by a video camera at 20 Hz (Fig. 2a, computer 2). Low-power 540 nm (0.1 mW mm^{-2}) epifluorescent illumination was used to visualize the neurons co-expressing light-gated ion channels and mKO[24] at ×15 by an EMCCD camera at 40 Hz (computer 1). Image thresholding and particle detection were used as the image-processing algorithms to identify the mKO-tagged neurons. As the animal swung its head, the neurons in the field rotated and changed their positions. To offset the rotation effect, positions of the neurons were measured using the principal axis and the distance from the centre of mass of the processed image. The processed images were then used to track the animal and to position the DLP mirrors to deliver light (4 mW mm^{-2}, 480 or 540 nm) on the neurons of interest with any desired temporal patterns to excite or inhibit the activity of the neurons. Feedback between the motorized stage, DLP mirrors and image-processing software was operated at 40 frames s^{-1} to achieve a 5-µm spatial resolution of excitation on a freely moving animal. The images were processed, recorded and analysed by customized LabView scripts.

Reversal frequency. L4-stage animals were transferred to a new NGM plate with a thin layer of *E. coli* OP50, containing 100 µM ATR if required, 24 h before experiments in room temperature. A 6-cm copper ring was placed in an open-lid, food-free 10 cm NGM plate immediately before the experiments to keep the animals in the field of view. Young adults were then transferred to the assay plate for 1 min before the experiment started. The desired wavelength of light (1 mW mm^{-2}, 480 or 540 nm) was delivered in alternate 3-min intervals for 1 h using customized LabView scripts. The experiments were recorded by a video camera at 20 Hz. Reversal frequency was calculated from pirouettes determined by an automated worm tracker (http://wormsense.stanford.edu/tracker)[25].

Virtual light gradient set-up. An AIY::*ChR2* animal was placed on an open-lid, food-free 10 cm NGM plate for at least 1 min before starting the experiment. A virtual gradient of light, $I(r) = \exp(-r^2/r_0^2)$, from 0 to 1 mW mm^{-2} over 1.3 mm, where $r_0 = 0.8$ mm, was defined in an x–y coordinate system tied to the centre of mass of the animal, which was always at the centre of the gradient profile (0.65 mm, 0.65 mm) (Supplementary Fig. 7a). The virtual light gradient moved with the centre of mass of the animal but at a fixed orientation. At each time (t), the coordinates of the nose tip were identified to calculate the corresponding intensity of light $I(n_x,n_y)$ (Fig. 4a). The animal was then illuminated with blue (480 nm) light at intensity $I(n_x,n_y)$, and thus AIY instantaneously experienced the intensity of light at the nose tip.

Molecular biology. *Arch::EGFP*[14] was cloned into the Fire Lab vector kit plasmid pPD96.52. *Chop-2(H134R)::TagRFP* was obtained by swapping red fluorescent protein *TagRFP* with yellow fluorescent protein (*YFP*) in the previously cloned *chop-2(H134R)::YFP*[16]. *Arch::TagRFP* and *Arch::mKO* were obtained, respectively, by swapping *TagRFP*[26] or *mKO*[24] with *EGFP* in *Arch::EGFP*. *TagRFP* and *GCaMP-3* (ref. 27) were codon-optimized for *C. elegans* (*de novo* synthesized by GenScript), whereas others were optimized for mammalian cells. We amplified 2 kilobases (kb) *str-2* (ref. 28), 1 kb *ttx-3* (ref. 29), 3 kb *npr-9* (ref. 30), 4.5 kb *ser-2prom2* (ref. 31) and 2.4 kb *odr-2(18)* (ref. 32) by PCR from *C. elegans* genomic DNA. All of the promoters were then fused with the desired light-gated ion channels by PCR fusion[33].

24. Karasawa, S., Araki, T., Nagai, T., Mizuno, H. & Miyawaki, A. Cyan-emitting and orange-emitting fluorescent proteins as a donor/acceptor pair for fluorescence resonance energy transfer. *Biochem. J.* **381,** 307–312 (2004).
25. Ramot D., Johnson B. E., Berry T. L. Jr, Carnell L. & Goodman M. B. The parallel worm tracker: a platform for measuring average speed and drug-induced paralysis in nematodes. *PLoS ONE* **3,** e2208 (2008).
26. Merzlyak, E. M. *et al.* Bright monomeric red fluorescent protein with an extended fluorescence lifetime. *Nature Methods* **4,** 555–557 (2007).
27. Hires, S. A., Tian, L. & Looger, L. L. Reporting neural activity with genetically encoded calcium indicators. *Brain Cell Biol.* **36,** 69–86 (2008).
28. Troemel, E. R., Sagasti, A. & Bargmann, C. I. Lateral signaling mediated by axon contact and calcium entry regulates asymmetric odorant receptor expression in *C. elegans*. *Cell* **99,** 387–398 (1999).
29. Hobert, O. *et al.* Regulation of interneuron function in the *C. elegans* thermoregulatory pathway by the *ttx-3* LIM homeobox gene. *Neuron* **19,** 345–357 (1997).
30. Bendena, W. G. *et al.* A *Caenorhabditis elegans* allatostatin/galanin-like receptor NPR-9 inhibits local search behavior in response to feeding cues. *Proc. Natl Acad. Sci. USA.* **105,** 1339–1342 (2008).
31. Tsalik, E. LIM homeobox gene-dependent expression of biogenic amine receptors in restricted regions of the *C. elegans* nervous system. *Dev. Biol.* **263,** 81–102 (2003).
32. Chou, J. H., Bargmann, C. I. & Sengupta, P. The *Caenorhabditis elegans odr-2* gene encodes a novel Ly-6-related protein required for olfaction. *Genetics* **157,** 211–224 (2001).
33. Boulin, T., Etchberger, J. F. & Hobert, O. Reporter gene fusions. *WormBook* (2006).